Synthesis of N-CNT-TiO_2 Nanocatalyst: Application in Direct Oxidation of H_2S to Sulfur

Daraee, Maryam; Baniadam, Majid*[+]

Chemical Engineering Department, Faculty of Engineering, Ferdowsi University of Mashhad, P.O. Box 91779-48974 Mashhad, I.R. IRAN

Rashidi, Alimorad*[+]

Nanotechnology Research Center, Research Institute of Petroleum Industry (RIPI), P.O. Box 14857-33111 Tehran, I.R. IRAN

Maghrebi, Morteza

Chemical Engineering Department, Faculty of Engineering, Ferdowsi University of Mashhad, P.O. Box 91779-48974 Mashhad, I.R. IRAN

ABSTRACT: *In this study, nitrogen-doped MWCNT-TiO_2 nanocatalyst (N-CNT-TiO_2) with 1, 3, and 5 wt. % nitrogen has been synthesized and its catalytic activity in the oxidation of H_2S to sulfur has been studied at a temperature of 200°C and O_2/H_2S mole ratio of 0.5 and compared with those of neat TiO_2 and TiO_2-CNT hybrid. Their structure, morphology, and chemical properties have been determined by N_2 adsorption-desorption isotherms, XRD, SEM, TEM, UV, and FT-IR. N-CNT-TiO_2 exhibited improved performance compared with TiO_2-CNT due to the presence of nitrogen groups. In addition, the nanocatalyst was comparable (up to 5%) with TiO_2 because of the presence of a lower bandgap and synergistic effects. Furthermore, 5%N-CNT-TiO_2 has shown the highest catalytic activity among N-CNT-TiO_2 nanocatalysts due to its higher surface area and pore volume.*

KEYWORDS: *N-CNT-TiO_2; Nanocatalyst; Nitrogen group; Catalytic activity.*

INTRODUCTION

Hydrogen sulfide (H_2S) is a poisonous gas which it is produced via many industrial processes such as natural gas, coal gasification and petrochemical plants. From the viewpoint of increasing the standards of efficiency (<7ppm) and environmental protection, the removal of H_2S from H_2S containing gases has become very important [1, 2]. The conventional H_2S removal method, which transforms H_2S into elemental sulfur, is the Claus process [3]. However, due to the thermodynamic retrictions of the Claus process, typical sulfur recovery efficiencies are only 90–95% for a two stage reactor [4]. Therefore, direct oxidation of H_2S to elemental sulfur is used for dilute H_2S containing gas streams [5,6].

Metal based [7-12] and carbon based [13-15] catalysts are used for removing H_2S in the direct oxidation process. Metal based catalysts perform better at relatively high

* *To whom correspondence should be addressed.*
+ E-mail: baniadam@um.ac.ir ; rashidiam@ripi.ir
1021-9986/2020/5/131-144 14/$/6.04

temperatures while carbon based catalysts are required for discontinues processes at lower temperatures [6]. Carbon material catalysts have various applications in catalytic [13, 16] or adsorptive [17] processes. The main disadvantage of carbon based catalysts is their poor selectivity at temperatures higher than 180°C [6, 13, 16]. On the other hand, the insertion of foreign elements into carbon networks has received great remarks during the past decade. Insertion of foreign elements could lead to the significant modification of their intrinsic properties [18-21].

Among the different carbon based catalysts, carbon nanotubes doped with nitrogen are used as catalysts and adsorbents due to the fact that their chemical and physical properties are strongly modified by nitrogen incorporation compared with pure carbon nanotubes. In fact, the acidic-basic properties are modified and the electronic surface state of the support is changed by nitrogen [22]. Nitrogen modifies the carbon and metal interaction with the deposited active phase and thus provides a new catalyst with better efficiency. Indeed, the insertion of nitrogen atoms into the hexagonal network structure of carbon seems to increase the density of the anchorage sites for active phase on the nanotube surface or depositing metal. That leads to the higher dispersion of the active phase nanoparticles and consequently a significant improvement of the overall catalytic activity compared to the undoped CNT [23, 24]. The main advantage of the N-CNT catalysts application against the traditional metal/metal oxide supported ones is that the nitrogen atoms are well anchored within the catalyst structure of the former and thus problems associated with the active phase sintering could be avoided [25].

Nitrogen doped Carbon NanoTubes (N-CNT) have been utilized in H_2S removal processes by various research groups [16, 26, 27]. N-CNTs is used for the selective oxidation of H_2S into elemental sulfur and exhibits better catalytic performance compared to Fe_2O_3/SiC and Fe_2O_3/SiO_2 at higher reactant gaseous velocity and lower reaction temperature [16]. Also, CNTs and N-CNTs is combined with TiO_2 in photocatalytic applications due wonderfull properties TiO_2 [28-31].

In our previous work, TiO_2-CNT hybrid nanocatalyst was synthesized and its activity in direct oxidation of H_2S to elemental sulfur was investigated and compared to that of TiO_2 [32]. In this work, TiO_2 was coated on N-CNT and the obtained composite was used as a catalyst for direct oxidation of H_2S to S at 200°C and with using mixture of O_2/H_2S in ratio equal to 0.5. The influence of nitrogen concentration in N-CNT-TiO_2 catalyst on the desulfurization activity and sulfur selectivity has been investigated and the results have been compared with those of TiO_2-CNT hybrid and TiO_2 catalysts.

EXPERIMENTAL SECTION

Materials

The starting materials for catalyst synthesis, including titanium tetra isopropoxide (TTIP) (99%), isopropanol, and nitric acid (65%), were supplied by Aldrich Chemical Company. Camphor (Merck Chemical Company), Urea (Merck Chemical Company) and Co-Mo/MgO, used as the growth catalyst, were provided by the Research Institute of Petroleum Industry (R.I.P.I.). Distillated water was used in all the experiments.

N-CNT synthesis procedure

N-doped multi-wall carbon nanotubes were synthesized via catalytic chemical vapor deposition of camphor, urea and Co-Mo/MgO [33] as the carbon source, nitrogen source and growth catalyst, respectively, under hydrogen atmosphere [27]. The reactions were carried out at 1000°C. Urea to camphor ratios were between 1-5 wt. %. The products are nominated to as N-CNT1 (1% nitrogen), N-CNT2 (3% nitrogen) and N-CNT3 (5% nitrogen). The treatment of N-CNTs was carried out in two stages: a) as-synthesized N-CNTs were placed in HCl for 24 h and then b) kept in HNO_3 acid for 6 h. The prepared samples were washed several times with distilled water to reach pH=7. Finally, the samples were dried at 80°C for 12 h in an oven. Synthesis process of N-doped CNT is shown in Fig. 1.

N-CNT-TiO_2 synthesis procedure

Various ratios of N-CNT-TiO_2 hybrid were synthesized according to the following procedure: N-CNT1 (1wt.%N-CNT), N-CNT2 (3wt.%N-CNT) and N-CNT-3 (5wt.%N-CNT) were added into a mixture of titanium tetra isopropoxide (TTIP) and isopropanol and the mixture was sonicated for 60 min. This solution was nominated as solution I. A certain amount of nitric acid and a specific volume of distilled water were mixed to achieve pH=1 and the obtained solution was nominated as solution II. Solution I was added dropwise to solution II

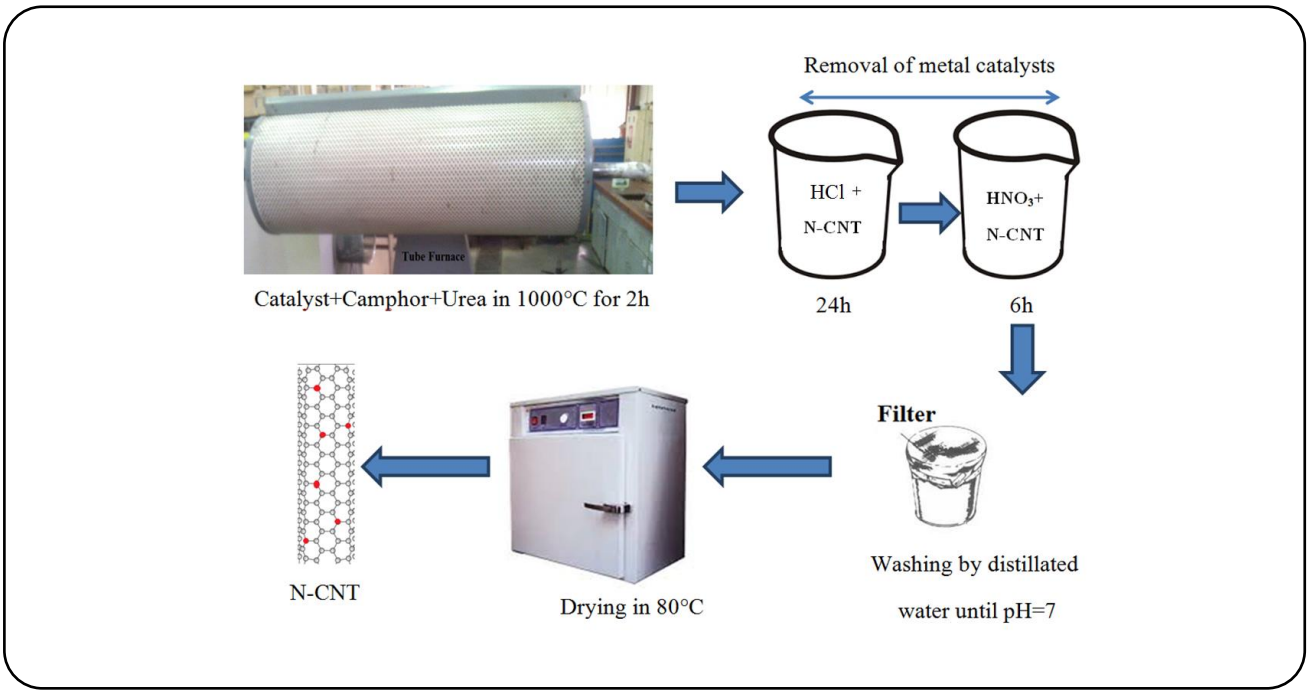

Fig.1: synthesis process of N- doped.

while the latter was being vigorously stirred. The resulting colloidal solution was blended for 2 h to produce a sol, which was then aged for 24 h in an ethylene glycol bath at 80°C and exposed to air for 24 h at ambient temperature to produce a gel. The samples were dried at 110°C for at least 12 h. Finally, the dried samples were calcined in a nitrogen gas atmosphere in a furnace at 400°C for 2 h. N-CNT-TiO_2 synthesis process is shown in Fig. 2.

Characterization of N-CNT-TiO_2

X-ray powder diffraction patterns are registered (XRD, BrukerAXS-D8 Advance X-ray diffractometer high- angle diffraction (10-80)) with Cu Kα radiation. Fourier transform infrared (FT-IR) spectra of catalysts were estimated by the KBr method recorded on a Perkin Elmer-Spectrum 65 from 4000 to 600 cm^{-1}. Nitrogen adsorption-desorption isotherms were obtained at 196°C using a Belsorp mini automatic adsorption instrument after degassing the samples at 150°C for 5h. Results of isotherms are specific surface area (S) with a Brunauer–Emmett–Teller (BET), V_t (total pore volume), V_{mic} (micropore volume). The morphology and particle size of the catalysts is approved by electron microscopy technique (FE-SEM, VEGA3 TE-SCAN instrument and TEM with Zeiss - EM10C - 80 KV).

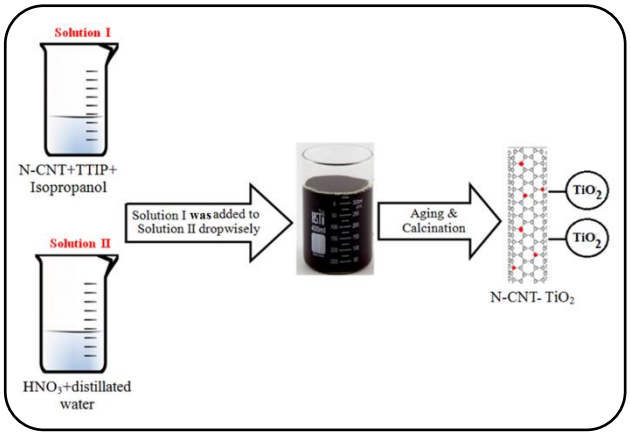

Fig. 2: Synthesis process of N-CNT-TiO_2.

Methods and measurements

Fig. 3 shows the experimental apparatus for the H_2S removal system. The set up consists of a gas supply unit, a fixed bed reactor in the vertical furnace, and a monitoring system for gas and temperature. The mixture of N_2, H_2S and O_2 gases adjusted by mass flow controllers, were passed through the fixed bed reactor. The reactor (1 cm of internal diameter and 50 cm of length) was filled with N-CNT-TiO_2 catalyst. In order to inhibit formation of a hot spot point within the catalyst bed, quartz glass is used. 10 g of the catalyst mixture (2 g of the catalyst and 8 g

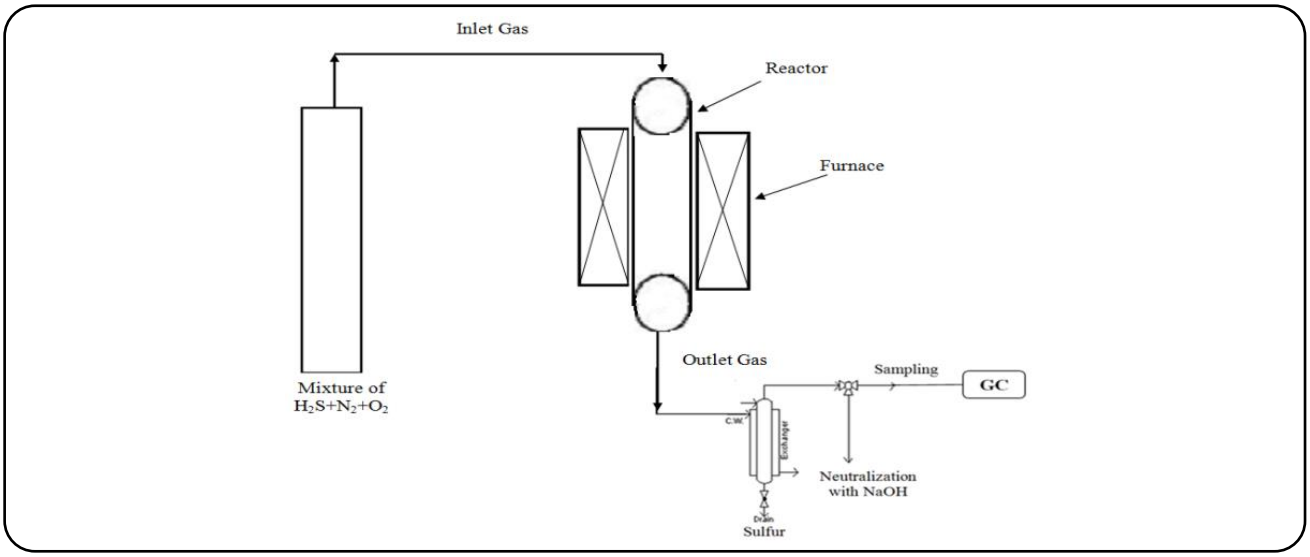

Figure 3: Lab-made apparatus for direct oxidation H_2S to S process.

of quartz glass with 30-60 mesh) were placed in the reactor, which was sealed by quartz wool from both sides. The H_2S and SO_2 concentrations in the reactor outlet were monitored using a gas chromatograph (Agilent 7890b). Equations 1, 2, and 3 show H_2S conversion, sulfur selectivity and yield, respectively.

$$H_2S\ Conversion = \frac{H_2S_{in} - H_2S_{out}}{H_2S_{in}} \quad (1)$$

$$Sulfur\ selectivity = \frac{H_2S_{in} - H_2S_{out} - So_{2out}}{H_2S_{in} - H_2S_{out}} \quad (2)$$

Sulfur yield= H_2S Conversion× Sulfur Selectivity (3)

RESULTS AND DISCUSSION

Chemical composition

FT-IR spectra approve various nitrogen bonds formed in the N-CNT structure. Different nitrogen types formed within the N-CNT structure; that is, N-H, C=N, and N-O, can be attributed to pyrrolic and pyridinic nitrogens and part of pyridinic oxide structure, respectively. All the graphitic, pyridinic and pyrrolic nitrogens have C-N bonds [34].

The absorption bonds of the synthetic N-CNTs are given in Fig. 4 (a, b and c). The FTIR spectrum of characteristic frequencies of pyrrolic N-H, graphitic C-N, pyridinic oxide of N-O and pyridinic nitrogen of C=N are observed for N-CNT1, N-CNT2 and N-CNT3, at 796, 1120, 1384 and 1629 cm^{-1}, respectively. *Ghasemy et al.* has reported the presence of nitrogen peaks [27]. It has been reported that pyridinic nitrogen provides basic sites with the highest catalytic activity for direct oxidation of H_2S to S due to its electron pair [13, 16]. In addition, the amount of pyridinic nitrogen formed in the N-CNT structure is one of the important parameters associated with catalytic properties. According to FT-IR analysis, peak intensity of nitrogen groups in 5%N-CNT is higher than other catalysts and it can related with better performance of 5%N-CNT than 1 and 3% N-CNT in H_2S oxidation [27].

Fig. 4 (d, e and f) shows the FT-IR spectrum of the synthetic N-CNT-TiO_2. The adsorbed water molecule peaks due to the stretching vibration of the hydrogen-bonded OH groups is seen in the range of 3000 to 3600 cm^{-1}. The FTIR spectrum of the nanomaterial shows a broad band below 950 cm^{-1}, which is assigned to inorganic Ti–O–Ti network [35]. Graphitic C-N at 1120 cm^{-1}, pyridinic oxide of N-O at 1384 cm^{-1} and pyridinic nitrogen of C=N at 1629 cm^{-1} are also observed. The characteristic peak of Ti-O-Ti is below 900cm^{-1} which it may overlap with pyrrolic nitrogen of N-H at 780 cm^{-1} and so, N-H peak disappeared. Also, the characteristic peak of adsorbed water molecules is around 1630cm^{-1} which it may overlap with pyridinic nitrogen of C=N at 1629 cm^{-1}. According to the FTIR results, all N-CNTs have pyridinic oxide or nitrogen, as previously indicated, which could represent their catalytic activity toward H_2S selective oxidation. The intense peaks reduced with the addition of TiO_2 to N-CNT in Fig. 5 which it show TiO_2 nanoparticles have been dispersed favorably on N-CNT. Also, peak intensity of nitrogen groups in 5%N-CNT-TiO_2 is higher than other

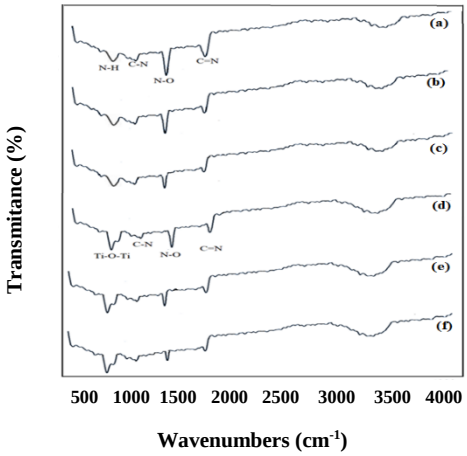

Fig. 4: FT-IR spectra of catalysts: a) N-CNT3, b) N-CNT2 , c) N-CNT1, d)5%N-CNT-TiO_2, e) 3%N-CNT-TiO_2 and f) 1%N-CNT-TiO_2.

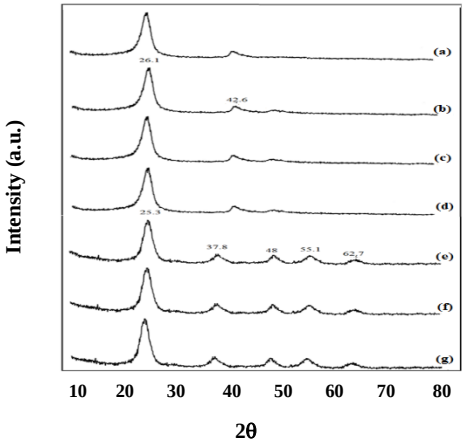

Fig. 6: XRD patterns of catalysts: a) MWCNT, b) N-CNT3, c) N-CNT2, d) N-CNT1, e) 5%N-CNT-TiO_2, f) 3%N-CNT-TiO_2 and g) 1%N-CNT-TiO_2.

catalysts and it can attribute to high performance of N-CNT-TiO_2 in H_2S oxidation.

Crystalline structure

The XRD patterns of the neat MWCNT and N-CNT in three different weight percentages of 1, 3 and 5 are shown in Fig. 6 (a,b, c and d). The main peaks at 26.1 and 42.6 are attributed to the (002) and (100) reflections of N-CNT, respectively, which show that the occupied N-CNT is a highly graphitized structure. The XRD patterns of different catalyst are completely similar [22].

The XRD patterns of the N-CNT-TiO_2 are shown in Fig. 7 (e, f and g). The peaks corresponding to N-CNT-TiO_2 hybrid, observed at 2θ of 25.3, 37.8, 48.0, 55.1, and 62.7°, can be ascribed to (101), (004), (200), (211), and (204) crystal planes, respectively [22]. These peaks are the anatase TiO_2 characteristic diffraction peaks. Notably, no N-CNT diffraction peaks are observed in the N-CNT-TiO_2 hybrid because the main characteristic peak of N-CNT has been overlapped by the main peak of anatase in N-CNT-TiO_2 hybrid [22]. Furthermore, the peaks associated with the growth catalyst are not observed in the XRD patterns [22]. The XRD patterns of different catalyst are completely similar.

The Raman spectrum of N-CNT-TiO_2 and N-CNT is showed in Fig. 7. TiO_2 anatase peaks are appeared at 145, 518 and 640 cm^{-1}. Two other predominant bands derived from 5%N-CNTs are appeared at 1378 and 1581 cm^{-1} which it could be attributed to the D- and G-bands of N-CNTs, respectively. The Raman spectra showed a clear increase in the intensity of the D-band for 5%N-CNT-TiO_2 compared to 5%N-CNTs, probably due to the influence of interaction between anatase TiO_2 and N-CNTs and the integration of TiO_2 in the N-CNT structure, which diminishes the ordering of the graphitic network [36, 37].

The TGA curves of 5%N-CNT and 5%N-CNT-TiO_2 are shown in Fig. 8. The weight losses of the 5%N-CNT and 5%N-CNT-TiO_2 are around 71% and 58%, which implies to thermal stability of 5%N-CNT-TiO_2 compared to 5%N-CNT. This higher thermal stability of 5%N-CNT-TiO_2 may be related to the presence of TiO_2 [36, 37].

Fig. 9 shows the UV-Vis diffuse reflectance for 5%, 3% and 1% N-CNT-TiO_2 and pure TiO_2. It can be observed that the 5%N-CNT-TiO_2 catalyst exhibits a stronger visible light absorption compared to other catalysts. In fact, the absorption edge changed towards the longer wavelength. Absorbance edge of TiO_2, 1% N-CNT-TiO_2, 3% N-CNT-TiO_2 and 5% N-CNT-TiO_2 nano catalysts are observed at 388, 405, 450 and 463 nm, respectively. Compared with TiO_2, the presence of nitrogen doped enhances the absorption in the whole visible light region for N-CNT-TiO_2 nanostructures. Furthermore, the absorption of N-CNT-TiO_2 nanocatalyst is higher than that of TiO_2, which might be attributed to the interaction between N-CNT and TiO_2. Investigations have been shown that the smaller the band gaps in an oxide have the faster the rate of dissociation and reactivity of hydrogen sulfide and the strength of the H_2S and oxide interactions depends on the size of the band gap in the oxide metal [38-41]. It is anticipated that the metal or metal

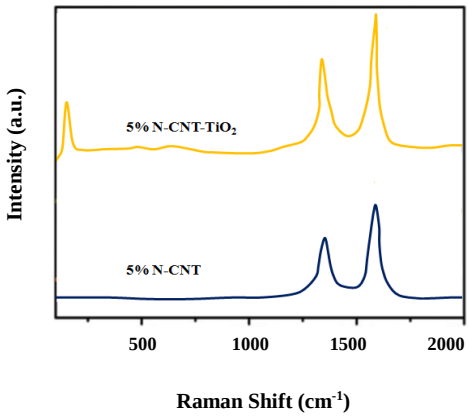

Fig. 7: Raman spectra of 5%N-CNT and 5%N-CNT-TiO_2.

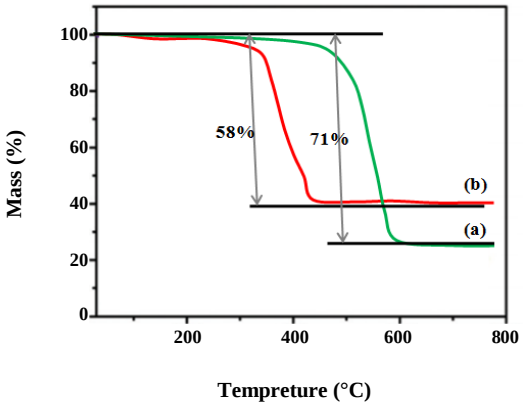

Fig. 8: TGA curves of a) 5%N-CNT and b) 5%N-CNT-TiO_2.

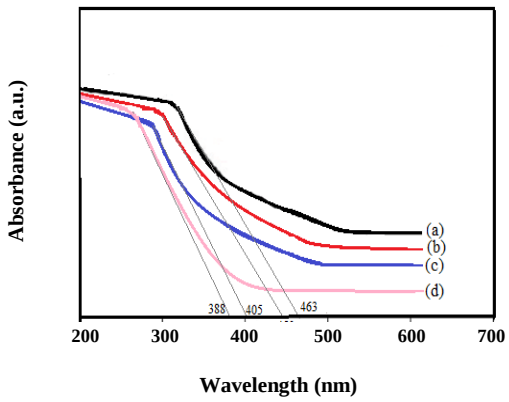

Fig. 9: UV analysis: a) 5%N-CNT-TiO_2, b)3%N-CNT-TiO_2, c) 1%N-CNT-TiO_2 and d) TiO_2.

oxide provides a large number of electronic states that can be very efficient for bonding interactions with S-containing molecules. Orbital mixing can explaine the effects of the band-gap size on the reactivity of an oxide and the behavior of metal oxide surfaces in the presence of S-containing molecules. When two orbitals are mixed, final orbital is lower in energy than the initial orbitals and another which is higher in energy. Band gap TiO_2 is high and when N-CNT is added to TiO_2, the absorption spectra N-CNT-TiO_2 has shifted towards the longer wavelength and the diagram slope has changed and is reduced bang gap due to synergetic effect and orbital mixing [42]. On the other hand, TiO_2 is an n-type semiconductor and incorporation with CNTs would lead the flow of electrons to the N-CNTs surfaces. So, the CNTs are acting as electron sinks and TiO_2 is converted to a p-type semiconductor. Here, electrons moved easily from the valence band to the conduction band of anatase TiO_2 due to reduction band gap with addition N-CNT [43]. Therefore, that N-CNTs doped TiO_2 are anticipated to have better performance than TiO_2 for direct oxidation H_2S to S and 5% N-CNT-TiO_2 is predicted to show the best performance in the direct oxidation of H_2S to S due to its smaller band gap.

In UV-VIS experimental method, a beam with a wavelength varying between 180 and 1100 nm passes through a solution in a cuvette. The one or more sample component absorbs this UV or visible radiation and then, we scan through various wavelengths in the UV/Vis region of the electromagnetic spectrum. Finally, data is plotted on curve. The x-axis (horizontal) shows the wavelength. The y-axis (vertical) shows the dependent variable the absorbance. We calculated the band gap from UV-Vis spectra of the samples. The band gap energy (Eg) can be obtained from UV spectrum by the following equation 4 [43]:

$$Eg=1239.8/\lambda \quad (4)$$

where Eg is the band gap energy (eV) and λ is absorption maximum wavelength (nm). The calculated maximum wavelength and band gap values are 463, 450, 405 and 388nm and 2.67, 2.71, 3.06 and 3.19 eV for 5% N-CNT-TiO_2, 3% N-CNT-TiO_2, 1% N-CNT-TiO_2 and TiO_2[32], respectively.

Surface area and morphology

Figs. 10 (a and b) and 11(a and b) show the BET surface area and BJH plot were done for 5, 3 and 1% N-CNT and N-CNT-TiO_2, respectively. In this work, total

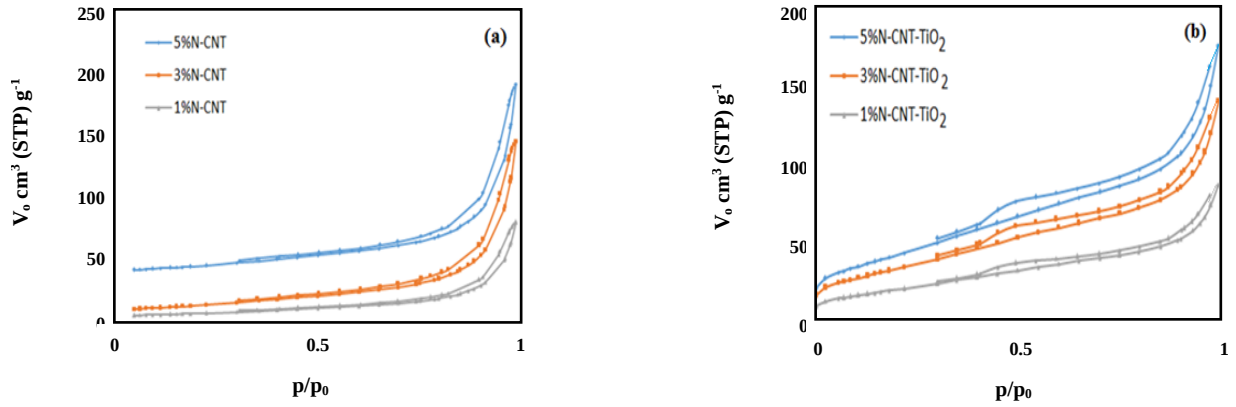

Fig. 10: The N_2 adsorption–desorption isotherms of catalysts: a) N-CNTs and b) N-CNT-TiO_2s.

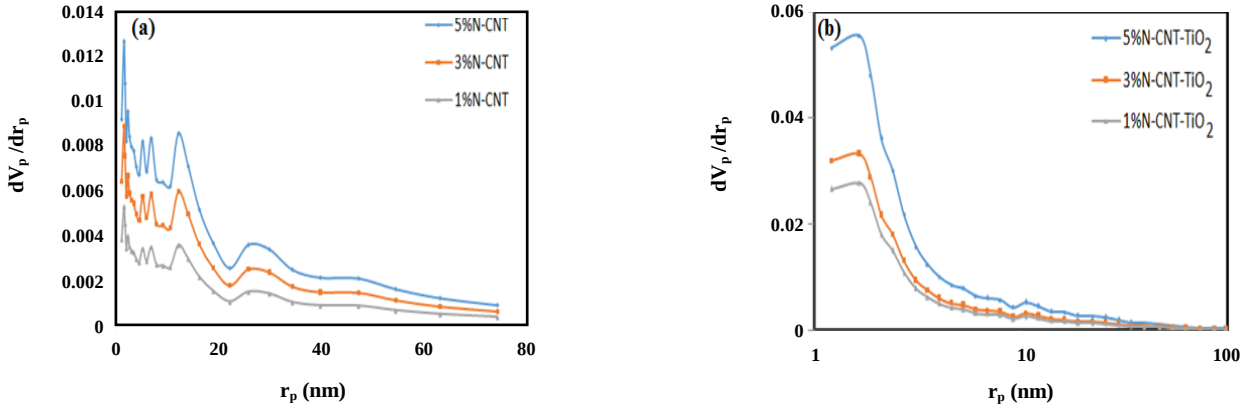

Fig. 11: BJH Plot of catalysts: a) N-CNTs and b) N-CNT-TiO_2s.

pore volume obtained from the amount adsorbed at P/P_0=0.99 and convert it to liquid volume by $4V_T/S_{BET}$ with an assumption that the pores are cylindrical.

The surface area was found of 5%, 3% and 1% N-CNT are 54, 43 and 22 m^2/g, respectively. It can be observed that there are some pores with inner hollow cavities and small diameter in various parts of N-CNT. Furthermore, the catalysts show type IV isotherms (including hysteresis loop) according to IUPAC classification, exhibiting that the synthesized catalysts are mesoporous with narrow pore texture. The BJH analysis indicates that the pore diameter is in the range of 17 to 20 nm for N doped CNTs. The pore size distribution of 5% N-CNT represents a higher degree of porosity than the other two catalysts.

The surface areas were measured of 5%, 3% and 1% N-CNT-TiO_2 are 154, 138 and 112 m^2/g, respectively. It can be observed that there are some pores with inner hollow cavities and small diameter in all of the N-CNT-TiO_2 catalysts. In addition, the catalysts show type IV isotherms according to IUPAC classification, exhibiting that the synthesized catalysts are mesoporous with narrow pore texture. The BJH analysis indicates that the pore diameter is in the range of 6 to 8nm for N-doped CNTs. The pore size distribution of 5% N-CNT-TiO_2 represents a higher degree of porosity than the other two catalysts. The interstitial space of N-CNT is anticipated to increase because of irregular nanoparticles of TiO_2 inserted into N-CNT network and the inhibition of agglomeration of N-CNT-TiO_2. This is in agreement with the FESEM analysis in Fig. 12 and the higher surface area in Fig. 10 for N-CNT-TiO_2 compared with N-CNT. Therefore, the addition of TiO_2 has led the hybrid catalyst to have a higher surface area than N-CNT. Table 1 exhibites the N_2 adsorption-desorption isotherms values for all of the catalysts.

Fig. 12 shows the FESEM and TEM images of bare 5% N-CNT and 5% N-CNT-TiO_2 hybrid, with outer diameters

Table 1: Surface area, pore volume and pore diameter measurements for all of the synthesized catalysts.

Catalyst	$a_{s,\ BET}$ (m^2/g)	Pore volume (cm^3/gr)	d(nm)
5%N-CNT	54	0.24	18.0
3%N-CNT	43	0.20	20.1
1%N-CNT	22	0.14	17.6
5%N-CNT-TiO_2	154	0.26	6.9
3%N-CNT-TiO_2	138	0.23	8.3
1%N-CNT-TiO_2	112	0.21	6.4
TiO_2-CNT[32]	304	0.28	3.8
TiO_2[32]	162	0.14	3.0

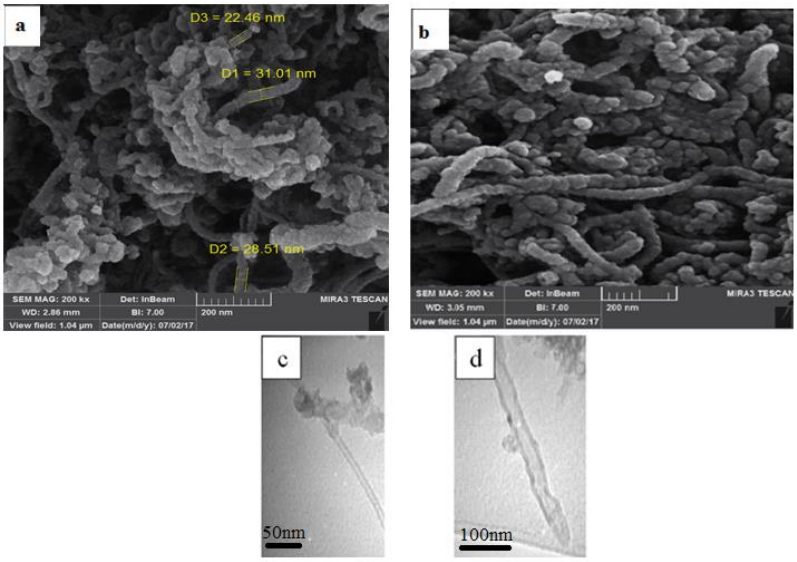

Fig. 12: FESEM micrograph of catalysts: a) 5%N-CNT, b) 5%N-CNT-TiO_2, c and d) TEM micrograph 5%N-CNT-TiO_2.

of 15-25 nm and 20-30 nm, respectively. The nanomaterial has a bamboo-like or tubular morphology with a relatively smooth surface. TiO_2 nanoparticles are almost uniformly coated on the surface of N-CNT in 5% N-CNT-TiO_2 and agglomeration phenomenon does not happen. In fact, the addition of TiO_2 to N-CNT maintains the initial morphology of the catalyst with tubular structure. The TEM image of 5% N-CNT-TiO_2 (Fig. 12 (c and d)) shows that it is fully coated with TiO_2 nanoparticles. The bamboo-like morphology of N-CNT-TiO_2 can also be clearly observed. The surface is entirely and homogeneously covered by TiO_2 nanoparticles. EDX spectrum presented in Fig. 13 further determined the existence of Ti, O, C and N atoms.

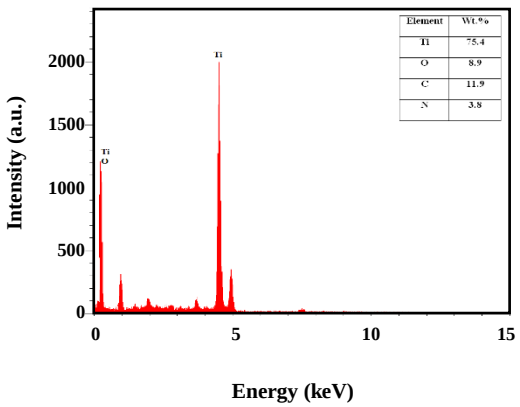

Fig. 13: EDX spectrum of 5%N-CNT-TiO_2.

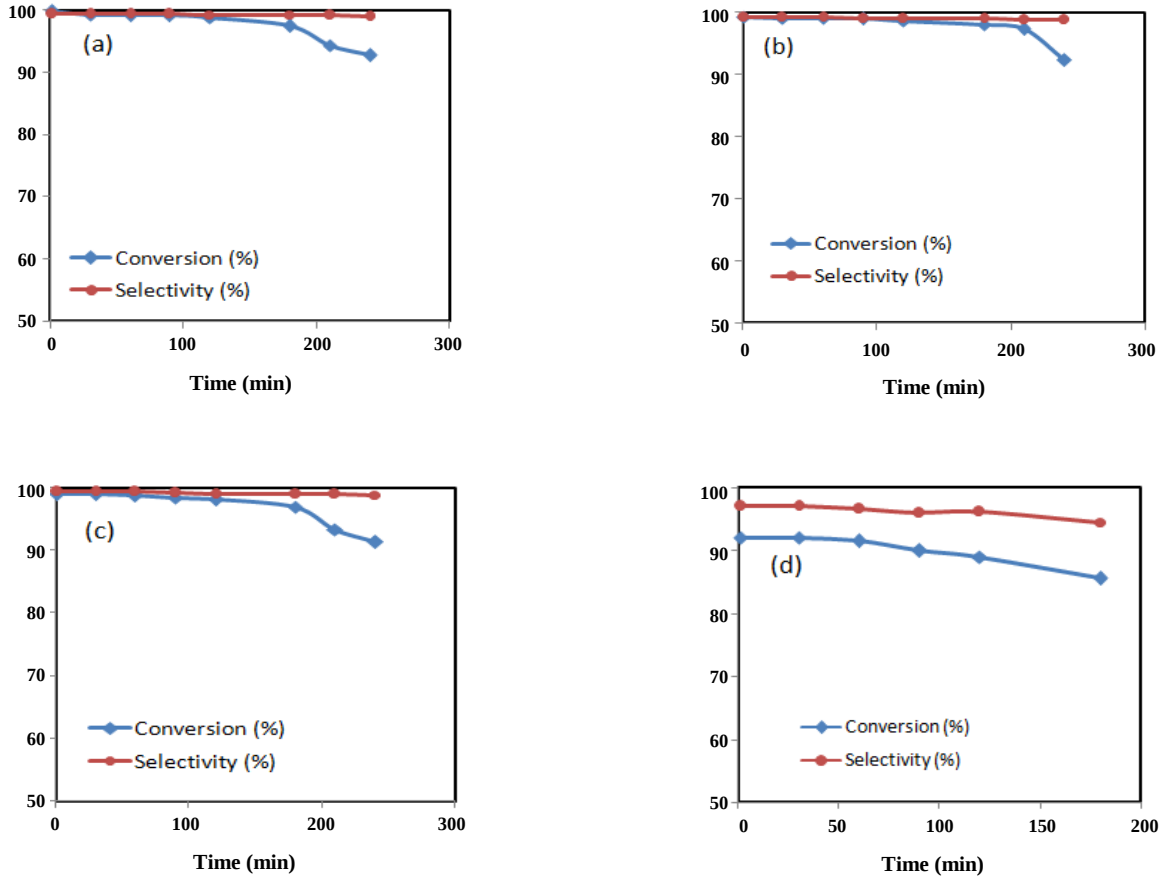

Fig. 14: Catalytic performance of a) 1%N-CNT-TiO_2, b) 3%N-CNT-TiO_2, c) 5%N-CNT-TiO_2 and d) 5%N-CNT for direct oxidation reaction in 200°C and O_2/H_2S ratio of 0.5.

Performance of N-CNT-TiO_2 in direct oxidation H_2S to S

Fig. 14 shows the performance of three N-CNT-TiO_2 catalysts with 1, 3 and 5 weight percentages of nitrogen in the selective oxidation of H_2S to S at the optimized temperature of 200°C, O_2/H_2S=0.5, for a 4400 ppm feed stream and GHSV of 35000 h^{-1}. The results demonstrate that the conversion decreases in the order of 5% N-CNT-TiO_2 (99.7%)> 3% N-CNT-TiO_2 (99.3%) > 1% N-CNT-TiO_2 (99%)> TiO_2-CNT (98.3)> TiO_2 (93.5%) > 5% N-CNT (92%). 5% N-CNT-TiO_2 catalyst with 99.7% of H_2S conversion gives the maximum conversion in 4 h reaction time. The selectivity of all the catalysts was more than 99%. This activity is higher than the value reported by previous investigations [16, 26]. According to our BET results, TiO_2 provides higher surface area for 5% N-CNT-TiO_2 compared to 5% N-CNT catalyst. The particle size of N-CNT in this sample is about 15-25 nm. However, when TiO_2 is coated on N-CNT, the size of N-CNT-TiO_2 increases to 20-30 nm, so increased surface area with addition TiO_2 to N-CNT. Also, It showed that the adsorption and reaction of H_2S on TiO_2 anatase (101) surfaces is easier than other phases due to lower energy barrier and the catalytic potential of TiO_2 nanoparticles for H_2S destruction efficiency is significant at high temperatures[44,45].

According to results, we compared the amount of nitrogenous compounds in different N-CNT catalysts (via FT-IR spectra) and is concluded that 5% N-CNT/TiO_2 present the best performance. Nitrogen species are the most active sites for H_2S selective oxidation due to their electron density, which provides basic centers for H_2S dissociation [13, 16]. In addition, the synergistic effects of TiO_2 and N-CNT may cause 5% N-CNT-TiO_2 to perform better than 3 and 1% N-CNT-TiO_2 and TiO_2. All the N-CNT-TiO_2 catalysts exhibit much higher activity in the direct oxidation reaction compared to the undoped TiO_2-CNT. 5% N-CNT-TiO_2

Table 2: Comparison of H_2S oxidation for various metal free catalysts.

Metal free catalyst	Conversion (%)	Selectivity (%)	Temperature (°C)	Reference
Nitrogen-Doped Carbon Composite	95	57	230	46
highly N-doped carbon phase macroscopic supports	99	72	210	47
Mesoporous nitrogen doped CNT	99.5 99.7	86.7 73.4	210 230	27
Mesoporous carbon spheres	100 Poor	100 Poor	Room temperature High temperature	48
N-CNT-TiO_2	99.7	99.5	200	In this article

has the highest activity due to its higher surface area and pore volume. The results show that H_2S is selectively oxidized at 200°C and O_2/H_2S ratio of 0.5 and there are no side reactions in the presence of 5% N-CNT/TiO_2 catalyst according Eq. (5).

$$H_2S + 0.5O_2 \xrightarrow{\text{single tep}} H_2O + S \quad (5)$$

For comparative purposes, recently cited data related to the sulfur capacities of various catalysts are listed in Table 2 for the oxidation of H_2S containing the major operational conditions for desulfurization processes. In spite of the differences in the experimental conditions, the H_2S conversion and sulfur selectivity of as-prepared nanocatalysts were higher than the results cited in the literature. Although it should be noted that due to the differences of experimental conditions, this comparison needs to be taken cautiously.

Mechanism of catalytic for H_2S removal

The XRD patterns of 5% N-CNT-TiO_2 before and after direct oxidation reaction time of 5 h are shown in Fig. 15. Fig. 16 show Scheme of possible catalytic mechanism of 5%N-CNT-TiO_2 catalyst.

The introduction of nitrogen enhances the hydrophilicity and alkalinity of the CNTs. The hydrophilicity of CNTs in the presence of humidity assists the formation of thin water film. Water is produced in the reaction in the form of steam. The alkalinity boosts the sorption and dissociation of H_2S into HS^- ions [50]. Then, elemental sulfur produced by oxidized of HS^- ions via O* at the active sites [50]. Sulfur is present in the form of steam at 200°C (above the dew point of sulfur). Since the boiling point in the pores is different from that on the catalyst surface, it is expected that the deposition of sulfur in the pores of mesoporous catalyst pursues the capillary condensation phenomena [49]. The catalyst is mesoporous and it includes small pore sizes. Thus, sulfur deposition on the catalyst surface causes the pores to plug and decreases the catalytic activity as a function of reaction time. In addition, there is no significant change in the particle size and phase of 5% N-CNT-TiO_2 catalyst after the reaction. This shows that the sintering phenomena may not have happened. The investigation indicated that nitrogen atoms are well anchored within the catalyst structure and thus problems associated with the active phase sintering are not observed [25]. Also, it showed that the adsorption and reaction of H_2S on TiO_2 anatase (101) surfaces is easier than other phases (rutile and brookit) due to lower energy barrier and the catalytic potential of TiO_2 nanoparticles for H_2S destruction efficiency is significant at high temperatures. So, it is suggested that the H_2S dissociation on N-CNT-TiO_2 surface resulting in formation of H_2O and S [44,45].

In order to investigate the catalytic performance, it is significant to elucidate the catalytic and deactivation mechanism of catalysts. Fig. 15 indicated schematic of deactivation 5%N-CNT and 5%N-CNT-TiO_2 catalyst by deposition of sulfur. XRD of 5 % N-CNT is compared before and after H_2S oxidation. It is predicted that deposition of sulfur in pores of mesoporous catalyst follow from capillary condensation phenomena. Sulfur is probably deposited in pore volume of N-CNT and N-CNT-TiO_2 catalyst and causes pore plugging. Therefore, the main reason of decreasing catalyst activity is sulfur deposition. However, XRD patterns of TiO_2 before and after use showed that the phase and particle size of N-CNT

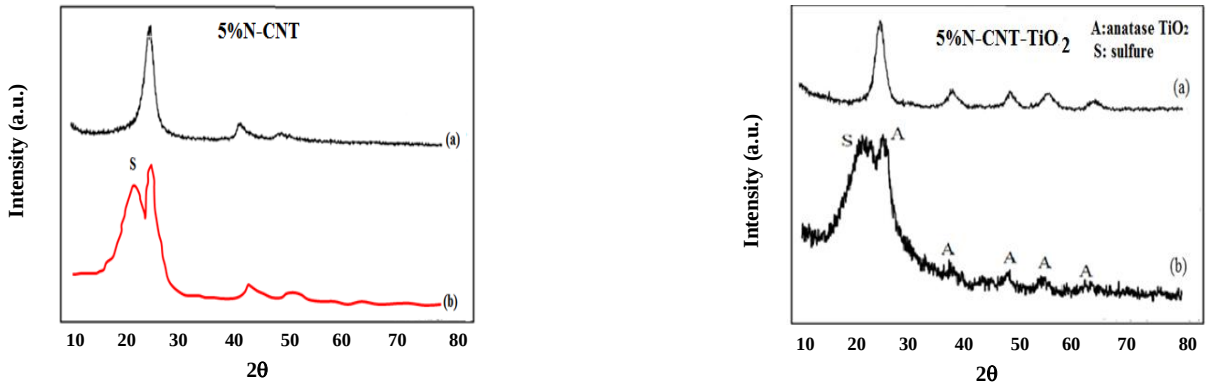

Fig. 15: XRD patterns 5%N-CNT and 5%N-CNT-TiO_2 a) before and b) after direct oxidation reaction time (5 h).

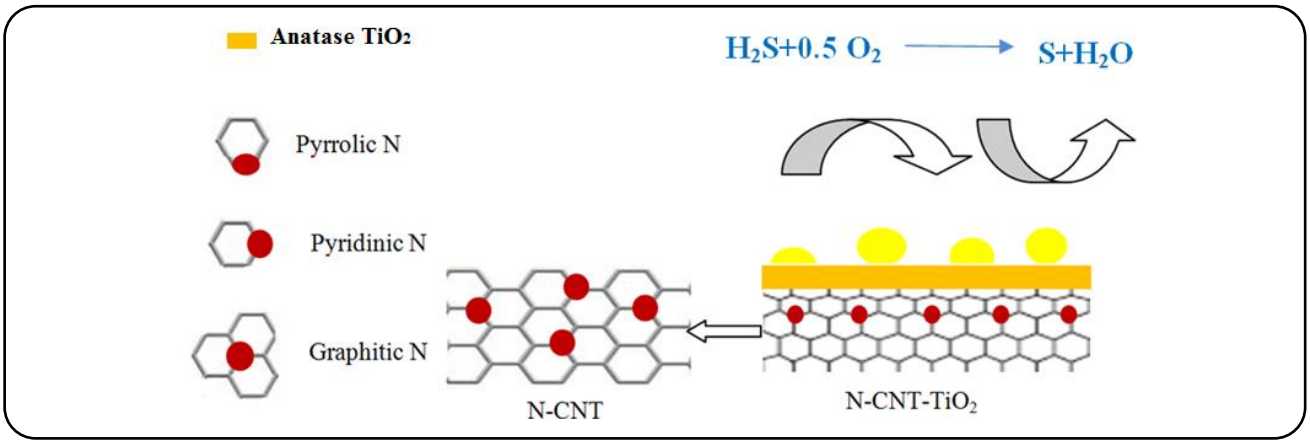

Fig. 16: Scheme of possible catalytic mechanism of 5%N-CNT-TiO_2 catalyst.

and N-CNT-TiO_2 had not changed after the reaction that has suggested that during oxidation considerable sintering don't took place due.

CONCLUSIONS

In this study, N-CNT-TiO_2 is compared with TiO_2-CNT hybrid and TiO_2 for removal H_2S in the reaction temperature of 200°C and O_2/H_2S ratio of 0.5. The structure, morphology and chemical properties of the catalysts have been determined by characterization techniques. FTIR and Raman analysis confirmed the presence of nitrogen groups; especially pyridinic and pyridinic oxide species and interaction N-CNT and anatase TiO_2 in the N-CNT-TiO_2 catalyst. The results showed that the insertion of nitrogen atoms into the CNT matrix significantly improved its chemical properties compared to the N free carbon nanotube-TiO_2 and TiO_2. All of the N-CNT-TiO_2 catalysts exhibit much higher activity in the direct oxidation reaction compared to the undoped ones. 5% N-CNT-TiO_2 has the highest activity (99.7%) due to its higher surface area and pore volume and lower band gap. It was revealed that all of the N-doped CNT with TiO_2 exhibited improved performance compared with TiO_2 due to the lower band gap and synergetic effect.

Received : Apr. 13, 2019 ; Accepted : Jul. 1, 2019

REFERENCES

[1] Ullah R., Bai P., Wu P., Liu B., Subhan F., Yan Z., Cation–Anion Double Hydroly- Sis Derived Mesoporous Mixed Oxides for Reactive Adsorption Desulfurization. *J. Microporous Mesoporous Mater*, **238**:36–45 (2017).

[2] Seredych M., Bandosz T.J., Desulfurization of Digester Gas on Catalytic Carbonaceous Adsorbents: Complexity of Interactions Between the Surface and Components of the Gaseous Mixture, *J. Ind. Eng. Chem. Res.*, **45**:3658-3665 (2006).

[3] Liu D., Wang Q., Wu J., Liu Y., A Review of Sorbents for High-Temperature Hydrogen Sulfide Removal from Hot Coal Gas, *J. Environmental Chemistry Letters*, **17**: 259-276 (2019).

[4] Ribeiro S.O., Juliao D., Cunha-Silva L., Domingues V.F., Valenca R., Ribeiro J.C., Catalytic Oxidative/Extractive Desulfurization of Model and Un- Treated Diesel Using Hybrid Based Zinc-Substituted Polyoxometalates, *J. Fuel*, **166**: 268–75 (2016).

[5] Tan R., Goltz R.H., Padilla G., Badhwar A.N., In Cross-Linked Macroptous Polymer Used for Selective Removal of Hydrogen Sulfide from a Gas Stream, US Patent App. 15/551,323, (2018).

[6] Zhang X., Tang Y., Qu S., Da J., Hao Z., H_2S-Selective Catalytic Oxidation: Catalysts and Processes, *J. ACS Catal*., **5**: 1053-1067 (2015).

[7] Reyes-Carmona A., Soriano M. D., Nieto J.M.L.P., Jones D.J., Jimenez-Jimenez J., Jimenez-Lopez A., Iron-Containing SBA-15 as Catalyst for Partial Oxidation Of Hydrogen Sulfide, *J. Catal. Today*, **210**: 117-123 (2013).

[8] Soriano M.D., Nieto J.M.L., Ivars F., Concepcion P., Rodriguez-Castellon E., Alkali-Promoted V_2O_5 Catalysts for the Partial Oxidation of H_2S to Sulphur, *J. Catalysis Today*, **192**: 28-35 (2012).

[9] Soriano M.D., Rodriguez-Castellon E., Garcia-Gonzalez E., Nieto J.M.L.P., Catalytic Behavior of Nav_6o_{15} Bronze for Partial Oxidation of Hydrogen Sulfide, *J. Catal. Today*, **238**: 62-68 (2014).

[10] Wang S.H., Wang Y.B., Dai Y.M., Jehng J.M., Preparation and Characterization of Hydrotalcite-Like Compounds Containing Transition Metal as a Solid Base Catalyst for the Transesterification, *J. Appl. Catal. A*, **439-440**: 134-141 (2012).

[11] Zhang X., Wang Z., Qiao N.L., Qu S.Q., Hao Z.P., Selective Catalytic Oxidation of H_2S over Well-Mixed Oxides Derived from $Mg_2Al_xV_{1-X}$ Layered Double Hydroxides, *J. ACS. Catal*, **4**: 1500-1510 (2014).

[12] Rezaee M., Kazemeini M., Fattahi M., Rashidi A.M., Vafajoo L., Oxidation of H_2S to Elemental Sulfur over Alumina Based Nanocatalysts: Synthesis and Physiochemical Evaluations, J. Scientia Iranica, *J. Transactions C: Chemistry and Chemical Engineering*, **23**: 1160-1174 (2016).

[13] Sun F., Liu J., Chen H., Zhang Z., Qiao W., Long D., Nitrogen-Rich Mesoporous Carbons: Highly Efficient, Regenerable Metal-Free Catalysts for Low-Temperature Oxidation of H_2S, *J. ACS. Catal*, **3**: 862-870 (2013).

[14] Xiao Y., Wang S., Wu D., Yuan Q., Catalytic Oxidation of Hydrogen Sulfide over Unmodified and Impregnated Activated Carbon, *J. Sep. Purif. Technol*, **59**: 326-332 (2008).

[15] Xiao Y., Wang S., Wu D., Yuan Q.J., Experimental and Simulation Study of Hydrogen Sulfide Adsorption on Impregnated Activated Carbon Under Anaerobic Conditions. *J. Hazard. Mater*, **153**:1193-1200 (2008).

[16] Chizari K., Deneuve A., Ersen O., Florea I., Liu Y., Edouard, D., Nitrogen-Doped Carbon Nanotubes as a Highly Active Metal-Free Catalyst for Selective Oxidation, *J. Chemsuschem*, **5**:102-108 (2012).

[17] Abbasabadi K., Rashidi A.M., Khodabakhshi S., Benzenesulfonic Acid-Grafted Graphene as a New and Green Nanoadsorbent in Hydrogen Sulfide Removal. *J. Natural Gas Science and Engineering*, **28**: 87-94 (2016).

[18] Yu D., Nagelli E., Du F., Dai L., Metal-Free Carbon Nanomaterials Become More Active Than Metal Catalysts and Last Longer, *J. Phys. Chem. Lett*, **1**: 2165-2173 (2010).

[19] Ayala P., Arenal R., Loiseau A., Rubio A., Pichler T., The Physical and Chemical Properties of Heteronanotubes, *J. Modern Physics*, **82**:1843-1885 (2010).

[20] Ba H., Viet C., Nhut Y.M., Granger P., Ledoux M.J., Huu C.P., Nitrogen-Doped Carbon Nanotube Spheres as Metal-Free Catalysts for the Partial Oxidation of H_2S, *J. Comptes Rendus Chimie*, **19**: 1303-1309 (2016).

[21] Yang Z., Liu Z., Zhang H., Yu B., Zhao Y., Wang H., N-Doped Porous Carbon Nanotubes: Synthesis and Application in Catalysis, *J. Chemical Communication*, (2017).

[22]Wang L., Shen L., Li Y., Zhu L., Shen J., Wang L., Enhancement of Photocatalytic Activity on Tio_2-Nitrogen-Doped Carbon Nanotubes Nanocomposites. *International Journal of Photoenergy*, (2013).

[23] Chizari K., Janowska I., Houlle M., Florea I., Ersen O., Romero T., Tuning of Nitrogen-Doped Carbon Nanotubes as Catalyst Support for Liquidphase Reaction, *J. Appl. Catal. A. Gen*, **380**: 72–80 (2010).

[24] Su D.S., Zhang J., Frank B., Thomas A., Wang X., Paraknowitsch J., Metal-Free Heterogeneous Catalysis for Sustainable Chemistry, *J. Chemsuschem*, **3**: 169-180 (2010).

[25] Duong-Vieta C., Truong-Phuoc L., Tran-Thanh T., Nhuta J.M., Nguyen-Dinh L., Janowska I., Nitrogen-Doped Carbon Nanotubes Decorated Silicon Carbide as Ametal-Free Catalyst for Partial Oxidation of H_2S, *J. Applied Catalysis A: General.* **482**:397–406 (2014).

[26] Ba H., Duong-Viet C., Liu Y., Nhut J.M., Granger P., Ledoux M.J., Nitrogen-Doped Carbon Nanotube Spheres as Metal-Free Catalysts for the Partial Oxidation of H_2S. *J. C. R. Chimie*, **19**: 1303-1309 (2016).

[27] Ghasemy E., Motejadded H.B., Rashidi A.M., Hamzehlouyan T., Yousefian Z., N-Doped CNT Nanocatalyst Prepared from Camphor And Urea for Gas Phase Desulfurization: Experimental and DFT Study, *J. Taiwan Institute of Chemical Engineers*, **85**: 121-131 (2018).

[28] Payan A., Fattahi M., Jorfi S., Roozbehani B., Payan S., Synthesis and Characterization of Titanate Nanotube/Single-Walled Carbon Nanotube (TNT/SWCNT) Porous Nanocomposite and Its Photocatalytic Activity on 4-Chlorophenol Degradation Under UV and Solar Irradiation, *J. Applied Surface Science*, **434:** 336-350 (2018).

[29] Payan A., Fattahi M., Roozbehani B., Jorfi S., Enhancing Photocatalytic Activity of Nitrogen Doped TiO_2 for Degradation of 4-Chlorophenol under Solar Light Irradiation, *Iranian Journal of Chemical Engineering (Ijche)*, **15**: 3-14(2018).

[30] Isari A.A., Payan A., Fattahi M., Jorfi S., Kakavandi B., Photocatalytic Degradation of Rhodamine B And Real Textile Wastewater Using Fe-Doped TiO_2 Anchored on Reduced Graphene Oxide (Fe-TiO_2/Rgo): Characterization and Feasibility, Mechanism And Pathway Studies, *J. Applied Surface Science*, **462**: 549-564 (2018).

[31] Hayati F., Isari A.A., Fattahi M., Anvaripour B., Jorfi S., Photocatalytic Decontamination of Phenol and Petrochemical Wastewater Through Zno/Tio_2 Decorated on Reduced Graphene Oxide Nanocomposite: Influential Operating Factors, Mechanism, and Electrical Energy Consumption, *J. RSC Advances*, **8**: 40035-40053 (2018).

[32] Daraee M., Baniadam M., Rashidi A.M., Maghrebi M., Synthesis Of Tio_2-CNT Hybrid Nanocatalyst and Its Application In Direct Oxidation of H_2S to S, *J. Chemical Physics*, **511**: 7-19 (2018).

[33] Rashidi A.M., Akbarnejad M.M., Khodadadi A.A., Mortazavi Y., Ahmadpour A., Single-Wall Carbon Nanotubes Synthesized Using Organic Additives to Co–Mo Catalysts Supported on Nanoporous MgO, *J. Nanotechnology*, **18**: 315-605 (2007).

[34] Wood K.N., Ohayrea R., Pylypenko S., Recent Progress on Nitrogen/Carbon Structures Designed for Use in Energy and Sustainability Applications, *J. Energy & Environmental Science*, 7: 1212 (2014).

[35] Khosravifard E., Salavati-Niasari M., Dadkhah M., Sodeifian G., Synthesis and Characterization of TiO_2-Cnts Nanocomposite and Investigation of Viscosity and Thermal Conductivity of a New Nanofluid, *J. Nano Structure*, **2**:191-197 (2010).

[36] Lin J., Ma D., Li Y., Zhang P., Mi H., Deng L., Suna L., Rena X.Z., In Situ Nitrogen Doping of TiO_2 by Plasma Enhanced Atomic Layer Deposition for Enhanced Sodium Storage Performance, *J. Dalton Trans.*, **46**:13101 (2017).

[37] Chizari K., Vena A., Laurentius L., Sundararaj U., The Effect of Temperature on the Morphology and Chemical Surface Properties of Nitrogen-Doped Carbon Nanotubes, *J. Carbon*, **68**: 369 –379 (2014).

[38] Rodriguez J.A., Chaturvedi S., Jirsak T., The Bonding of Sulfur to Pd Surfaces: Photoemission and Molecular–Orbital Studies, *J. Chemical Physics Letters*, **296**:421-428 (1998).

[39] Rodriguez J.A., Chaturvedi S., Kuhn M., Herbek J., Reaction of H_2S and S_2 with Metal/Oxide Surfaces: Band-Gap Size and Chemical Reactivity. *J. Phys. Chem*, **102**: 5511-5519 (1998).

[40] Rodriguez J.A., Jirsak T., Freitag A., Hansonjohn J.C., Chaturvedi Z.L.,. Interaction of SO_2 with CeO_2 and Cu/Ceo_2 Catalysts: Photoemission, XANES and TPD Studies, *J. Catalysis Letters*, **62**: 113-119 (1999).

[41] Rodriguez J.A., Maiti A., Adsorption and Decomposition of H_2S on Mgo(100), Nimgo(100), and Zno(0001) Surfaces: a First-Principles Density Functional Study, *J. Phys. Chem. B*, **104**: 3630-3638 (2000).

[42]Https://Chemistry.Stackexchange.Com/Questions/51636/Lowering-Energy-In-Molecular-Orbital-Mixing.

[43] Soroodan Miandoab E., Fatemi Sh., Upgrading TiO_2 Photoactivity under Visible Light by Synthesis of MWCNT/TiO_2 Nanocomposite, *Int. J. Nanosci. Nanotechnol*., **11**: 1-12 (2015).

[44] Huang W.F., Chen H.T., Lin M.C., Density Functional Theory Study of the Adsorption and Reaction of H_2S on TiO_2 Rutile (110) and Anatase (101) Surfaces, *J. Phys. Chem. C*, **113**: 20411–20420 (2009).

[45] Shahzad M., Hussain S.T., Ahmed N., Use of Pure and Sulfur Doped TiO_2 Nanoparticles for High Temperature Catalytic Destruction of H_2S Gas, *J. Chalcogenide Letters*, **10**:19 – 26 (2013)**.**

[46] Liu Y., Viet C.D., Luo J., Hébraud A., Schlatter G., Ersen O., Nhut J.M., One-Pot Synthesis of a Nitrogen-Doped Carbon Composite by Electrospinning as a Metal-Free Catalyst for Oxidation of H_2S to Sulfur, *J. Chem Cat Chem*, 2957-2964 (2015).

[47] Ba H., Liu Y., Phuoc L.T., Viet C.D., Mu X., Doh W.H., Thanh T.T., Baaziz W., Dinh L.N., Nhut J.M., Janowska I., Begin D., Zafeiratos S., Granger P., Tuci G., Giambastiani G., Banhart F., Ledoux M.J., Huu C.P., A Highly N-Doped Carbon Phase "Dressing" of Macroscopic Supports for Catalytic Applications, *J.C hem. Commun.*, **51**: 14393-14396 (2015).

[48] Zhang Z., Wang J., Li W., Wang M., Qiao W., Long D., Ling L., Millimeter-Sized Mesoporous Carbon Spheres for Highly Efficient Catalytic Oxidation of Hydrogen Sulfide at Room Temperature, *J. Carbon*, **96**: 608-615 (2016).

[49] Https://Www.Researchgate.Net/Post/How Does Capillary Condensation Affect Catalytic Activity of a Surface.

[50] Chen Q., Wang J., Liu X., Zhao X., Qiao W., Long D., Ling L., Alkaline Carbon Nanotubes as Effective Catalysts for H_2S Oxidation, *J. Carbon*, **49**: 3773-3780 (2011).